

**Di-hadron angular correlation function in event-by-event ideal hydrodynamics**

R. P. G. Andrade\* and J. Noronha†

*Instituto de Física, Universidade de São Paulo, Caixa Postal 66318, 05315-970 São Paulo, São Paulo, Brazil*

(Received 21 May 2013; published 27 September 2013)

The di-hadron angular correlation function is computed within boost-invariant, ideal hydrodynamics for Au + Au collisions at  $\sqrt{s_{NN}} = 200$  GeV using Monte Carlo Glauber fluctuating initial conditions. When  $0 < p_T < 3$  GeV, the intensity of the flow components and their phases,  $\{v_n, \Psi_n\}$  ( $n = 2, 3$ ), are found to be correlated on an event-by-event basis to the initial condition geometrical parameters  $\{\varepsilon_{2,n}, \Phi_{2,n}\}$ , respectively. Moreover, the fluctuation of the relative phase between trigger and associated particles,  $\Delta_n = \Psi'_n - \Psi_n^a$ , is found to affect the di-hadron angular correlation function when different intervals of transverse momentum are used to define the trigger and the associated hadrons.

DOI: [10.1103/PhysRevC.88.034909](https://doi.org/10.1103/PhysRevC.88.034909)

PACS number(s): 12.38.Mh, 24.10.Nz, 25.75.Gz, 25.75.Ld

**I. INTRODUCTION**

The nontrivial structures in di-hadron angular correlation measurements with respect to a single charged (or neutral) high- $p_T$  trigger observed in heavy ion collisions [1–4] are among the most important probes of the hot and dense matter created in these reactions. In fact, angular correlations measured in Au + Au collisions at the BNL Relativistic Heavy Ion Collider (RHIC) with the center-of-mass energy per nucleon pair  $\sqrt{s_{NN}} = 200$  GeV are significantly different than those observed in  $pp$  or  $d + Au$  collisions (this difference, however, seems to disappear for the higher energy collisions performed at the CERN Large Hadron Collider (LHC) [5,6]). In the longitudinal direction, the di-hadron correlation function is characterized by a long-range structure in the relative pseudorapidity coordinate denominated “ridge” [3] while in the azimuthal direction one finds three prominent peaks: the near side peak  $\Delta\phi = 0$  aligned with the trigger hadron and two other away side peaks that are symmetrically positioned with respect to  $\Delta\phi = \pi$ . This azimuthal profile indicates the existence of a considerable fraction of higher order harmonic flows, mainly triangular and quadrangular flows, in addition to the well-known direct and elliptic flows.

These angular correlations have been studied in the past in the context of the energy deposited by jets in a smooth hydrodynamic medium [7–16]. In Refs. [17–19] it was suggested that the higher order harmonic flows are connected to the fluctuations in the initial conditions for hydrodynamics. In Ref. [19], it was shown that the fluctuations in the initial conditions, characterized by longitudinal tubelike structures, can in fact produce after hydrodynamic expansion the structures observed in the data.

Considerable effort has since been made towards understanding how harmonic flow components evolve from the initial geometry of the fluctuating initial conditions [20–26] to the final spectrum of observed particles. In other words, the elliptic flow,  $v_2$ , would be mostly created by the so-called participant eccentricity [27],  $\varepsilon_2$ , and the triangular flow,  $v_3$ ,

would be mostly created by the participant triangularity [20],  $\varepsilon_3$ , and so on.

It has been observed for Monte Carlo Glauber initial conditions that the Fourier coefficients  $v_2$  and  $v_3$  show a strong linear dependence with the respective eccentricities  $\varepsilon_2$  and  $\varepsilon_3$  [28,29]. However, similar results are not generally observed for higher Fourier coefficients such as, for instance,  $v_4$  and  $v_5$  [26,30]. It is important to mention that hydrodynamics, which is widely used to connect the initial conditions to the final spectrum of particles, does not guarantee such a linear response to the initial geometry due to intrinsic nonlinearities present in the hydrodynamic equations.

The aim of this article is to improve the current understanding of the role played by the higher order flow components in the determination of the azimuthal profile of the di-hadron correlation function in heavy ion collisions. The azimuthal component of this function can be parametrized in terms of the Fourier coefficients of the azimuthal distribution of particles; i.e., it can be described in terms of the pair  $\{v_n, \Psi_n\}$  where the first parameter is related to the intensity of the flow component and the second one is an angle that fixes the orientation of the respective harmonic. In particular, we are interested in the situation where the set of triggers is not identical to the set of associated particles, because it occurs when the triggers and the associated particles are defined within different ranges of transverse momentum. In this situation, as we are going to show in Sec. II, the di-hadron correlation function becomes particularly sensitive to not only the  $v_n$  coefficients but also the  $\Psi_n$  angles. More precisely, it depends on the relative phase  $\Delta_n = \Psi'_n - \Psi_n^a$ , where the first angle is computed using the triggers and the second using the associated particles. Recently, the fluctuation of this relative phase has been studied in  $3 + 1$  ideal hydrodynamics by the NexSPheRIO Collaboration [31] and also in  $2 + 1$  viscous hydrodynamics in Refs. [32,33]. In particular, in this article we try to understand the width of the  $\Delta_n$  distribution in terms of the geometry of the initial conditions. More precisely, we compute the distribution of the difference  $\delta_n = \Psi_n - \Phi_{2,n}$  (in three ranges of  $p_T$ ) to quantify the fluctuation of the flow component phase with respect to the geometrical orientation angle  $\Phi_{2,n}$ , obtained from the initial energy density distribution (in Sec. III the definition of the geometric parameters from the initial conditions is discussed). For instance, for Au + Au collisions at  $\sqrt{s_{NN}} = 200$  GeV, it

\*rone.andrade@gmail.com

†noronha@if.usp.br

was shown in Ref. [34] that the  $\delta_n$  distribution, for integrated  $p_T$ , is quite narrow (when  $n > 1$ ). Here, as we show, the study of this distribution for triggers and associated particles can be used to understand the behavior of the  $\Delta_n$  distribution. To complete the analysis involving flow and initial geometry, we also compute the correlation between the eccentricities  $\varepsilon_{2,n}$  and the flow parameters  $v_n$  for different bins of transverse momentum.

This paper is organized as follows. In Sec. II we describe the parametrization of the di-hadron angular correlation function in terms of the Fourier coefficients of the azimuthal distribution of hadrons. In Sec. III we discuss the definition of the eccentricities used in this paper. In Sec. IV we give the details about our hydrodynamic model including the modeling of the fluctuating initial conditions, the equation of state, and the decoupling mechanism. We discuss our results in Sec. V and we finish in Sec. VI with our conclusions. We use a mostly minus metric signature (+, -, -, -) and natural units  $\hbar = k_B = c = 1$ .

## II. FOURIER DECOMPOSITION OF THE DI-HADRON ANGULAR CORRELATION FUNCTION

The azimuthal component of the di-hadron correlation function,  $C(\Delta\phi)$ , can be defined as follows

$$C(\Delta\phi) = \frac{\langle \int g^a(\phi_t + \Delta\phi) g^t(\phi_t) d\phi_t \rangle}{\langle \int g^t(\phi_t) d\phi_t \rangle}, \quad (1)$$

where the functions  $g^t$  and  $g^a$  are the azimuthal distributions of triggers and the associated particles in each event, respectively. Each function is associated with an interval of transverse momentum  $p_T$ . The brackets indicate the average over events (an arithmetic mean). The denominator, naturally, is the average number of triggers.

The decomposition of Eq. (1) in terms of the Fourier coefficients of the azimuthal distribution of hadrons can be obtained using the following expansions:

$$g^a(\phi_t + \Delta\phi) = v_0^a + \sum_n 2v_0^a v_n^a \cos[n(\phi_t + \Delta\phi - \Psi_n^a)] \quad (2)$$

and

$$g^t(\phi_t) = v_0^t + \sum_m 2v_0^t v_m^t \cos[m(\phi_t - \Psi_m^t)]. \quad (3)$$

Observe that the values of the parameters  $\{v_n, \Psi_n\}$ , for both triggers and associated particles, vary from event to event.

Inserting the expansions (2) and (3) into Eq. (1), a straightforward calculation leads to the following general formula for the di-hadron correlation function in the azimuthal direction:

$$C(\Delta\phi) = c_0 + \sum_n c_n \cos(n\Delta\phi) + \sum_n \tilde{c}_n \sin(n\Delta\phi), \quad (4)$$

where

$$c_0 = \frac{\langle v_0^a v_0^t \rangle}{\langle v_0^t \rangle}, \quad (5)$$

$$c_n = \frac{2}{\langle v_0^t \rangle} \langle v_0^a v_0^t v_n^a v_n^t \cos[n(\Psi_n^t - \Psi_n^a)] \rangle, \quad (6)$$

and

$$\tilde{c}_n = \frac{2}{\langle v_0^t \rangle} \langle v_0^a v_0^t v_n^a v_n^t \sin[n(\Psi_n^a - \Psi_n^t)] \rangle. \quad (7)$$

Considering the simplest case in which the ranges of transverse momentum for both triggers and associated particles are the same, i.e., the case in which  $\Psi_n^t = \Psi_n^a$ , these equations tell us that the profile of the di-hadron correlation function depends only on the  $v_n$  coefficients, while the odd coefficients,  $\tilde{c}_n$ , are identically null.

On the other hand, when the ranges of transverse momentum for triggers and associated particles are different,  $\Psi_n^t \neq \Psi_n^a$ , the following questions can be posed:

- (i) What is the profile of the distribution of the relative phase ( $\Psi_n^t - \Psi_n^a$ ) as a function of the transverse momentum and centrality?
- (ii) Is the relative phase independent of the  $v_n$  coefficients? In other words, can we consider

$$c_n \approx c_n^f = \frac{2}{\langle v_0^t \rangle} \langle v_0^a v_0^t v_n^a v_n^t \rangle \langle \cos[n(\Psi_n^t - \Psi_n^a)] \rangle \quad (8)$$

when the number of events is sufficiently large (and similarly for the  $\tilde{c}_n$  coefficients)? The index  $f$  in Eq. (8) indicates the factorization of the  $c_n$  coefficient. Note that, even when this factorization is valid, the average over the cosine still needs to be determined.

It must be mentioned that in the well-known event plane method [35]  $\Psi_n^t = \Psi_n^a = \Psi_n^{\text{EP}}$  regardless of the  $p_T$  bin chosen for the trigger and associated hadrons, which means that the relative phase in this case is identically zero and, consequently, the di-hadron correlation function is necessarily an even function of  $\Delta\phi$ . However, in the case where the triggers and associated particles are defined within different  $p_T$  bins, there is no reason to assume that  $\Psi_n^t$  and  $\Psi_n^a$  are aligned in every single event. On the contrary, it is more natural to suppose that the relative phase fluctuates from event to event. In this scenario, considering that the relative phase distribution shows a peak at the origin  $\Delta_n = 0$  with some width, the main question becomes how far from the unit the absolute value of the factor  $\cos[n(\Psi_n^t - \Psi_n^a)]$  is. As one can see in Eq. (6), this factor can change the di-hadron angular correlation profile.

When the number of events is sufficiently large one expects that factorization can be used in Eqs. (6) and (7), and the resulting factor  $\langle \sin[n(\Psi_n^a - \Psi_n^t)] \rangle$ , related with the odd coefficient, is expected to average to zero. This means that the relative phase distribution becomes an even function in this limit and, thus, the parity of the di-hadron correlation function  $C(\Delta\phi)$  is restored.

## III. ECCENTRICITY DEFINITION

To quantify the anisotropy of the initial conditions event by event, in this article we use the following definition for the eccentricities:

$$\varepsilon_{m,n} = \frac{\{r^m \cos[n(\phi - \Phi_{m,n})]\}}{\{r^m\}}, \quad (9)$$

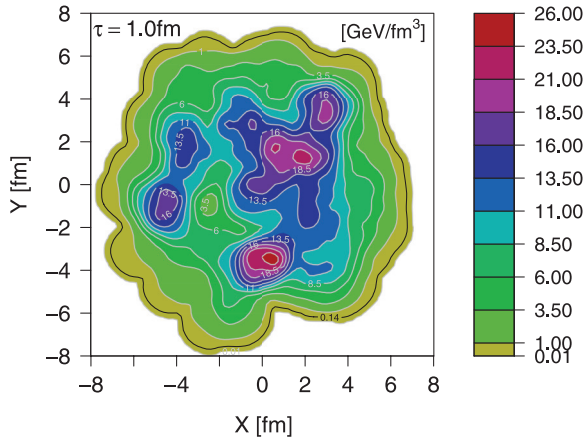


FIG. 1. (Color online) Initial energy density distribution in the transverse plane at the midrapidity for a randomly chosen Au + Au collision at 200 GeV in the 0–5% centrality class, computed using an implementation of the Monte Carlo Glauber model developed in Refs. [40,41].

where  $\{\dots\}$  indicates the average weighted by the energy density profile  $\epsilon(\vec{r})$  (see Fig. 1) in the transverse plane. The corresponding orientation angle is given by

$$\Phi_{m,n} = \frac{1}{n} \tan^{-1} \left( \frac{\{r^m \sin(n\phi)\}}{\{r^m \cos(n\phi)\}} \right). \quad (10)$$

Finally,  $r^m = (x^2 + y^2)^{\frac{m}{2}}$  and  $\phi = \tan^{-1}(y/x)$ .

The index  $m$  can be conveniently chosen to improve the prediction of the respective flow component. For instance, in Ref. [26], in the context of the NexSPheRIO code [36], it was shown that the triangular flow,  $v_3$ , is better predicted using  $m = 3$ . However, in this article we follow the original proposal in Ref. [20] and fix  $m = 2$ . We choose the solution of Eq. (10) that makes the eccentricity  $\epsilon_{2,n}$  a positive quantity. For instance, the phase  $\Phi_{2,2}$  corresponds to the major axis of the ellipse. It is easy to verify that  $\epsilon_{2,2}$  is the well-known participant eccentricity [27] in a coordinate system where  $\{x\} = \{y\} = 0$ . Thus,

$$\epsilon_{2,2} = \frac{\sqrt{(\sigma_x^2 - \sigma_y^2)^2 + 4\sigma_{xy}^2}}{\sigma_x^2 + \sigma_y^2}, \quad (11)$$

where  $\sigma_x^2 = \{x^2\}$ ,  $\sigma_y^2 = \{y^2\}$ , and  $\sigma_{xy}^2 = \{xy\}^2$ .

A motivation for definition (9) can be found in Ref. [24] where it was shown that the eccentricities defined above are related to the irreducible components of the cumulant expansion of the initial energy density distribution.

Given the eccentricities and their respective orientation angles, some interesting questions can be posed:

- (i) Do the Fourier coefficients,  $v_n$ , show a linear dependence on the respective eccentricity,  $\epsilon_{2,n}$ , independently on the transverse momentum range and centrality?
- (ii) Are the angles  $\Phi_{2,n}$  and  $\Psi_n$  aligned?

As was mentioned in the previous section, Eqs. (6) and (7) show that the  $v_n$  coefficients alone (or, equivalently, the eccentricities alone) do not provide enough information to produce the azimuthal structures observed in the di-hadron

correlation function [2] in the case where the  $p_T$  bins of the triggers and associated hadrons are different. For instance, in an extreme case in which the relative phases are randomly distributed, the di-hadron correlation function would not show any structure independently on the value of the  $v_n$  coefficients. In this context, a partial alignment between the orientation angle  $\Phi_{2,n}$  and the phase  $\Psi_n^a$  (see, for instance, Ref. [34]), as well as a partial alignment between  $\Phi_{2,n}$  and  $\Psi_n^t$ , would indicate a partial alignment between the angles  $\Psi_n^a$  and  $\Psi_n^t$ .

#### IV. DETAILS OF THE HYDRODYNAMIC MODELING

In this work, we use a (2 + 1) (i.e., boost-invariant [37]) ideal relativistic fluid to study the connection between the initial conditions and final flow observables relevant to the description of the di-hadron angular correlation function. We are focusing on the transverse expansion near midrapidity. In practice, we consider only a thin transverse slice of matter, so that  $|y| < 0.12$ , where  $y$  is the rapidity. To solve the ideal hydrodynamic equations, we apply the relativistic version of the so-called smoothed particles hydrodynamics (SPH) approach originally developed in Ref. [38], which is a suitable tool to deal with irregular distributions of matter (details about the SPH method and a discussion of how the ideal fluid nonlinear partial differential equations are solved within this approach are given in Appendix A). We assume that the baryon chemical potential is zero. Moreover, the initial transverse velocity is set to zero. Our code matches the previous tests made using the NexSPheRIO code [36] and, in Appendix B, we show that our code is able to perfectly match the exact solution of 2 + 1 ideal hydrodynamics obtained in Ref. [39] (also known as Gubser flow).

To get an idea of the type of energy density profiles obtained in event-by-event simulations, we show in Fig. 1 the initial energy density distribution in the transverse plane at the midrapidity for a randomly chosen central Au + Au collision at 200 GeV, computed using an implementation of the Monte Carlo Glauber model developed in Refs. [40,41] and used throughout this work. Note that this distribution is quite irregular, showing several regions where the energy is considerably concentrated (the so-called hot spots). Because the initial anisotropy in this model arises basely from the random position of the incident nucleons, the regions where the energy is concentrated correspond to the regions where the nucleon density is large. There is a normalization factor associated with the initial energy density distribution, which is chosen through a comparison to data. We set this factor so that the maximum of the average temperature distribution, in the 0–5% centrality window, coincides with the temperature of 0.31 GeV (similar values can be found in the literature; see, for instance, Ref. [42]). Once fixed by the central collisions, this overall factor is kept the same for the peripheral collisions studied in this work.

We use equation of state (EOS) S95n-v1 [43] in our model, which combines results from lattice QCD at high temperatures and the hadron resonance gas equation at low temperatures. The decoupling mechanism is based on the Cooper-Frye prescription [44]. In this approach, the particles become free after crossing a hypersurface of constant temperature,

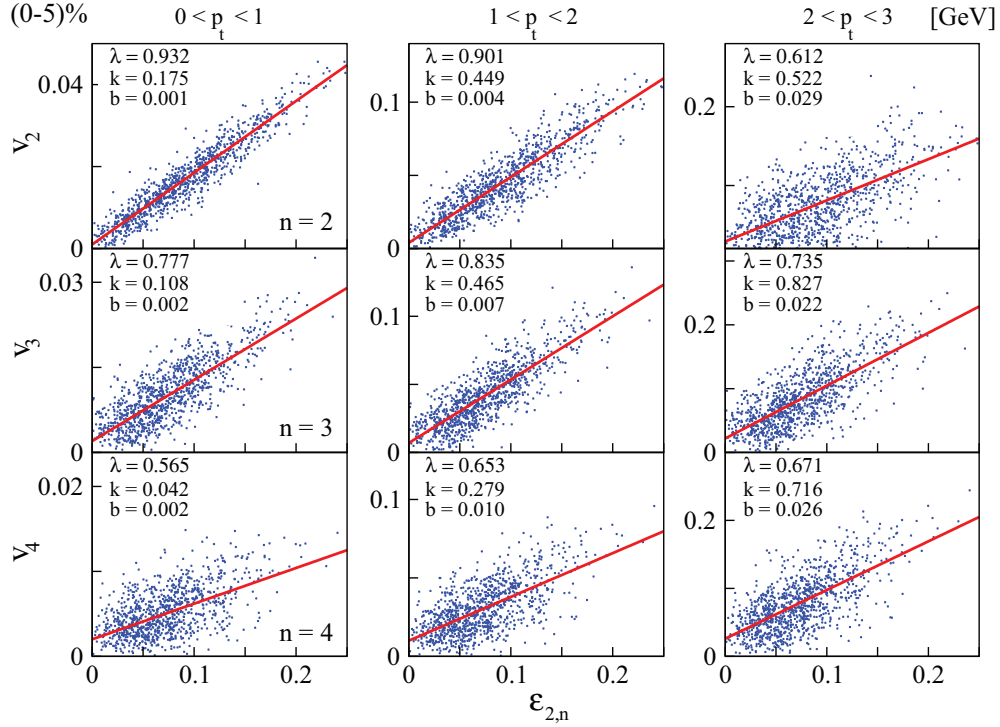


FIG. 2. (Color online) Correlation between the initial eccentricity,  $\epsilon_{2,n}$  ( $n = 2, 3, 4$ ), and the respective harmonic coefficient,  $v_n$ , in the 0–5% centrality window with 1000 events. Three ranges of transverse momentum are presented. The parameters  $k_n$  and  $b_n$  are obtained from the linear fit:  $v_n = k_n \epsilon_{2,n} + b_n$ . The parameter  $\lambda_n$  is the linear correlation coefficient [see Eq. (12)].

denominated freeze-out temperature  $T_{fo}$  (the details about the Cooper-Frye prescription in the SPH approach are discussed in Appendix C). In our hydrodynamic code, we have not implemented the decay of particles yet. All the results presented in this article correspond then to direct positively charged pions.

Because the goal of this article is not to make a rigorous comparison between our numerical results and the data but rather to understand how the flow components create the structures observed in the di-hadron correlation function, the role of the freeze-out temperature here is just to determine the expansion time of the fluid. By using  $T_{fo} = 0.14$  GeV, which is a typical value in the literature (see, for instance, Ref. [42]), the total expansion time in the 0–5% centrality window is around 15 fm. Proportionally, in the 20–30% centrality window, the expansion time is shorter,  $\sim 10$  fm. In both centrality windows studied in this article, the expansion time is sufficiently long to induce the hydrodynamic effects in the final spectrum of hadrons.

The initial time at which we begin the hydrodynamic evolution is  $\tau_0 = 1$  fm. In this work, the smoothing SPH parameter is chosen to be  $h = 0.3$  fm (see the discussion in Appendix A), which allows for relatively quick computation times while still preserving the important structure present in the initial conditions.

Summarizing, the procedure to compute an observable in a single event is the following: (i) Monte Carlo Glauber initial conditions are used to obtain the initial energy density in the transverse plane; (ii) the hydrodynamic evolution is calculated using the SPH method [38], and (iii) the final spectra is computed using the Cooper-Frye prescription [44]. At the end

of the simulation, the average value of a given observable is calculated over an ensemble of events. All the results presented in this article correspond to Au + Au collisions at  $\sqrt{s_{NN}} = 200$  GeV and 1000 events were computed.

## V. RESULTS

In Fig. 2 we show the correlation between the initial eccentricity,  $\epsilon_{2,n}$  ( $n = 2, 3, 4$ ), and the respective flow coefficient,  $v_n$ , in the 0–5% centrality window (central). A similar graph is shown in Fig. 3, in the 20–30% centrality window (peripheral). The parameters  $k_n$  and  $b_n$  are obtained from the linear fit:  $v_n = k_n \epsilon_{2,n} + b_n$ . Moreover,

$$\lambda_n = \frac{\langle (\epsilon_{2,n} - \langle \epsilon_{2,n} \rangle)(v_n - \langle v_n \rangle) \rangle}{\sqrt{\langle (\epsilon_{2,n} - \langle \epsilon_{2,n} \rangle)^2 \rangle \langle (v_n - \langle v_n \rangle)^2 \rangle}} \quad (12)$$

is the linear correlation coefficient. The closer to the unit  $|\lambda_n|$  is, the stronger the linear correlation between the variables  $\epsilon_{2,n}$  and  $v_n$  becomes. In fact, when  $\lambda \sim 1$  ( $\lambda \sim -1$ ) both variables show a strong linear correlation (anticorrelation).

One can see that the coefficients  $v_2$  and  $v_3$  are considerably correlated (linear correlation) with respect to the eccentricities  $\epsilon_{2,2}$  and  $\epsilon_{2,3}$ , respectively. This behavior is observed in almost all cases—for high transverse momentum particles ( $2 < p_t < 3$  GeV), in the 0–5% centrality window, the parameter  $\lambda_2$  is smaller in comparison to the other cases ( $\lambda_2 = 0.612$ ). In particular,  $\lambda_2$  obtained in the 20–30% centrality window is closer to the unit in comparison to the same parameter obtained in the 0–5% centrality window, due to the almondlike

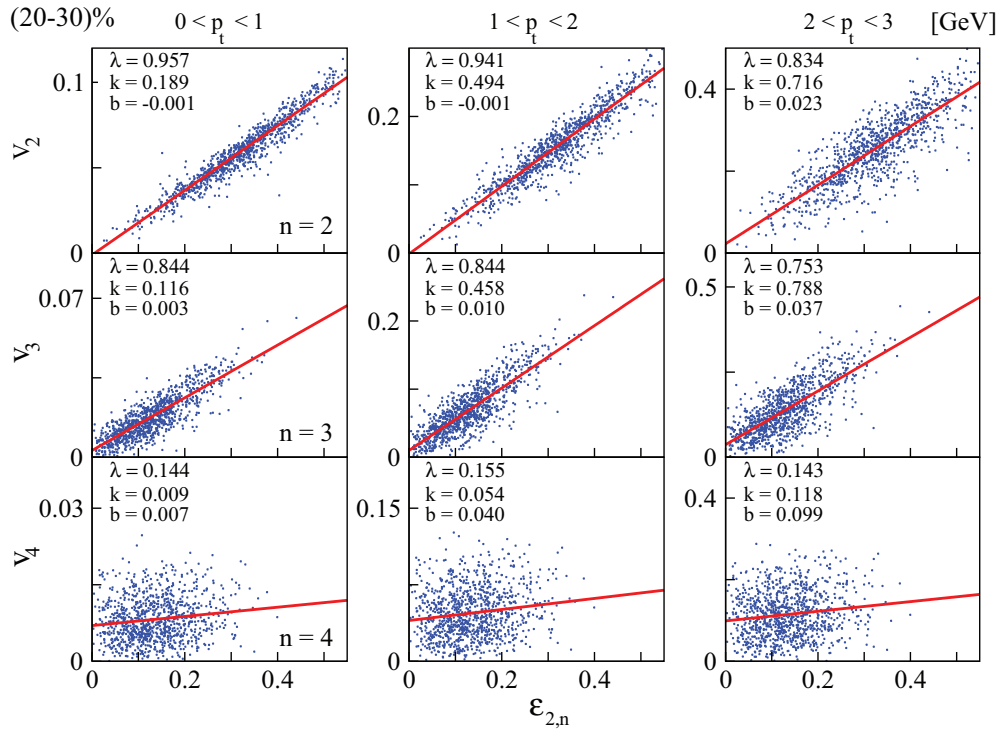


FIG. 3. (Color online) Correlation between the initial eccentricity,  $\epsilon_{2,n}$  ( $n = 2, 3, 4$ ), and the respective harmonic coefficient,  $v_n$ , in the 20–30% centrality window with 1000 events. Three ranges of transverse momentum are presented. The parameters  $k_n$  and  $b_n$  are obtained from the linear fit:  $v_n = k_n \epsilon_{2,n} + b_n$ . The parameter  $\lambda_n$  is the linear correlation coefficient [see Eq. (12)].

transverse shape of the initial conditions in the peripheral window, which produces stronger elliptic flow.

On the other hand,  $\lambda_3$  is less sensitive to centrality, which supports the idea that  $\epsilon_{2,3}$  is driven by fluctuations. This shows that the almond shape of the initial conditions in the 20–30% centrality window does not interfere with the correlation between  $\epsilon_{2,3}$  and  $v_3$ . Finally, the linear correlation between  $\epsilon_{2,4}$  and  $v_4$  is weaker, especially for peripheral collisions. These results are compatible with those obtained in Ref. [29] where the linear correlation between the  $p_T$  integrated flow coefficients and the eccentricities was investigated (within viscous hydrodynamics).

In Fig. 4 we show the distribution of the angular difference  $\delta_n = \Psi_n - \Phi_{2,n}$  ( $n = 2, 3, 4$ ) in the 0–5% centrality window. Note that  $\Psi_n$  is rotated by  $\pi/n$  to achieve the smallest angular difference with respect to  $\Phi_{2,n}$ . Four ranges of transverse momentum are presented. A similar graph is shown in Fig. 5 for the 20–30% centrality window. All distributions are normalized to 1. The vertical dashed line indicates the maximal difference for each harmonic, i.e.,  $\delta_n^{\max} = \pi/n$ . These results show that there is a partial alignment between the initial reference angle  $\Phi_{2,n}$  and the flow angle  $\Psi_n$  in almost all of cases. For high transverse momentum particles ( $2 < p_t < 5$  GeV), in the 0–5% centrality window, the difference  $\delta_2$  is broader in comparison to the remaining cases.

Note that the almondlike transverse shape of the initial conditions in the 20–30% centrality window produces a stronger elliptic flow that reduces the fluctuation of the angle  $\Psi_2$  with respect to the reference angle  $\Phi_{2,2}$ , making the distribution of the difference  $\delta_2$  narrower. On the other

hand, this mechanism does not influence the partial alignment between  $\Psi_3$  and  $\Phi_{2,3}$ , which is quantified by the width of the distribution of the difference  $\delta_3$ , i.e., in both centrality windows  $\delta_3$  is narrow. With respect to the fourth harmonic,  $\Psi_4$  and  $\Phi_{2,4}$  show a partial alignment as well (event though the linear correlation between  $v_4$  and  $\epsilon_{2,4}$  is weak).

Now we come to the study of the phase difference between triggers and associated hadrons. In Fig. 6 the distribution of the relative phase  $\Delta_n = \Psi_n^t - \Psi_n^a$  ( $n = 2, 3, 4$ ) is shown for the 0–5% centrality window. Three ranges of transverse momentum for associated particles are presented. A similar graph is shown in Fig. 7 for the 20–30% centrality window. All distributions are normalized to 1. The vertical dashed line indicates the maximal difference for each harmonic, i.e.,  $\Delta_n^{\max} = \pi/n$ . The range of transverse momentum for the triggers is defined as  $3 < p_t^{\text{trigg}} < 5$  GeV. In Ref. [45] a similar observable was employed to investigate the granularity of the initial conditions.

These results show that there is also a partial alignment between the angles  $\Psi_n^t$  and  $\Psi_n^a$ . Starting from the left and going to the right side in these plots, the distribution of the difference  $\Delta_n$  tends to be narrower once the kinematic region of the associated particles gets close to the kinematic region of the triggers. However, when both kinematic regions are far from each other, for instance, by choosing the associated particles with low transverse momentum ( $0 < p_t^a < 1$  GeV), this distribution can become considerably broad. This is the case for the  $\Delta_2$  distribution computed in the 0–5% centrality window. As we shall show below, this behavior makes the factor  $\cos[2(\Psi_2^t - \Psi_2^a)]$  deviate significantly from the unit. In contrast, the same distribution is narrow in the 20–30%

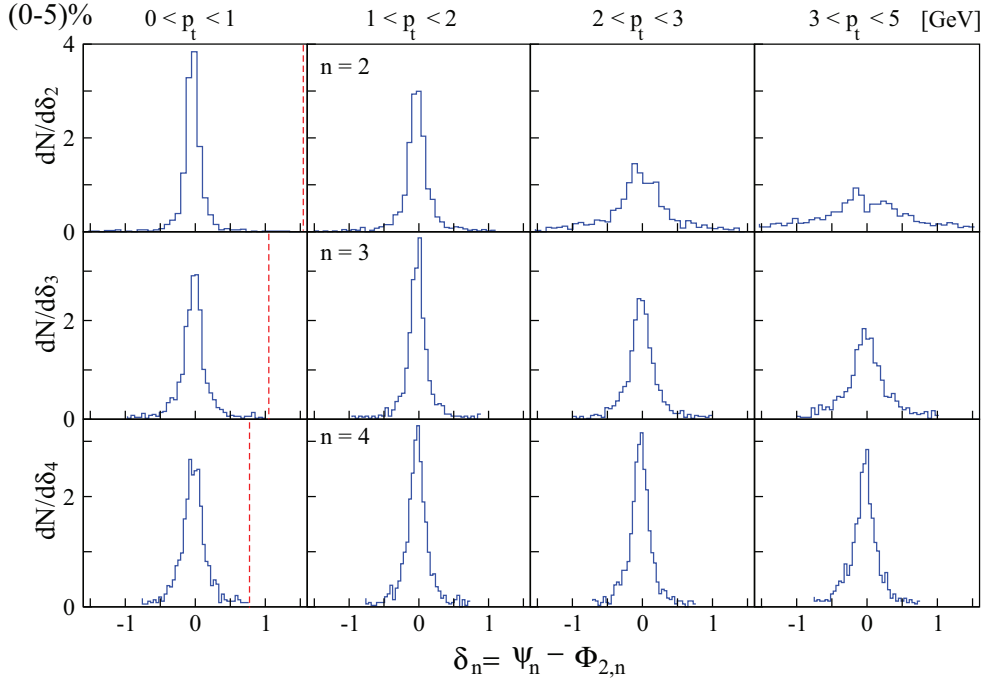


FIG. 4. (Color online) Distribution of the angular difference  $\delta_n = \Psi_n - \Phi_{2,n}$  ( $n = 2, 3, 4$ ) in the 0–5% centrality window with 1000 events. Four ranges of transverse momentum are presented. All distributions are normalized to 1. The vertical dashed line indicates the maximal difference for each harmonic, i.e.,  $\delta_n^{\max} = \pi/n$ .

centrality window. This behavior can be understood in terms of the geometry of the initial conditions. For instance, in Fig. 4 one can see that the difference  $\delta_2$  for the triggers is broad while the same distribution for the associated particles is narrow,

which means that  $\Psi_2^a$  and  $\Psi_2^t$  are not always aligned. For the remaining cases (with  $0 < p_t^a < 1$  GeV), the relative phase distribution is narrower because both angles are better aligned with the reference angle.

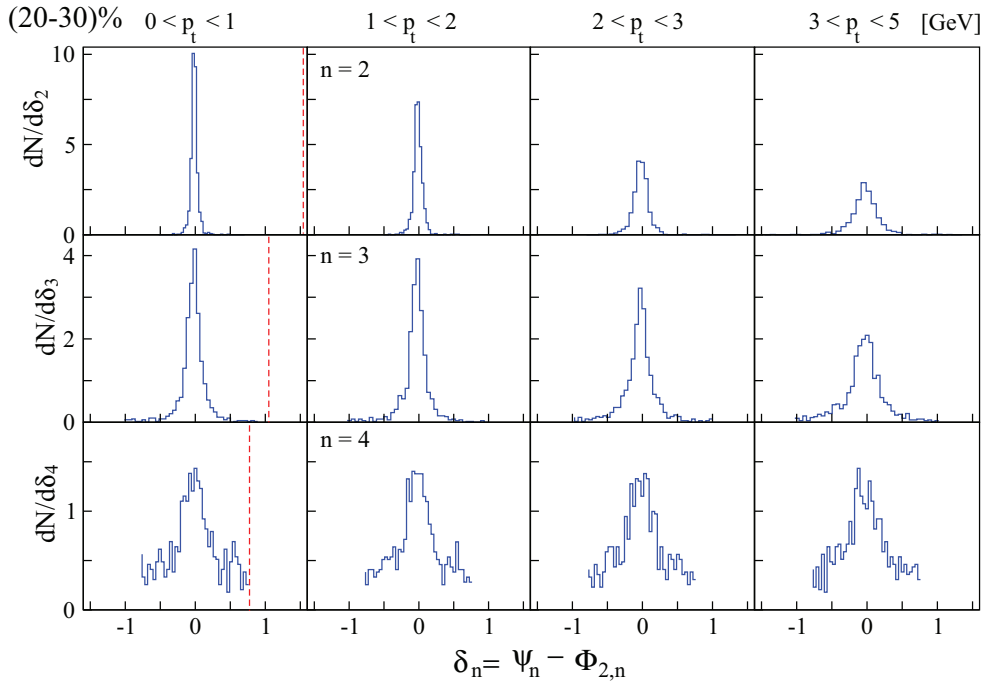


FIG. 5. (Color online) Distribution of the angular difference  $\delta_n = \Psi_n - \Phi_{2,n}$  in the 20–30% centrality window with 1000 events. Four ranges of transverse momentum are presented. All distributions are normalized to 1. The vertical dashed line indicates the maximal difference for each harmonic, i.e.,  $\delta_n^{\max} = \pi/n$ .

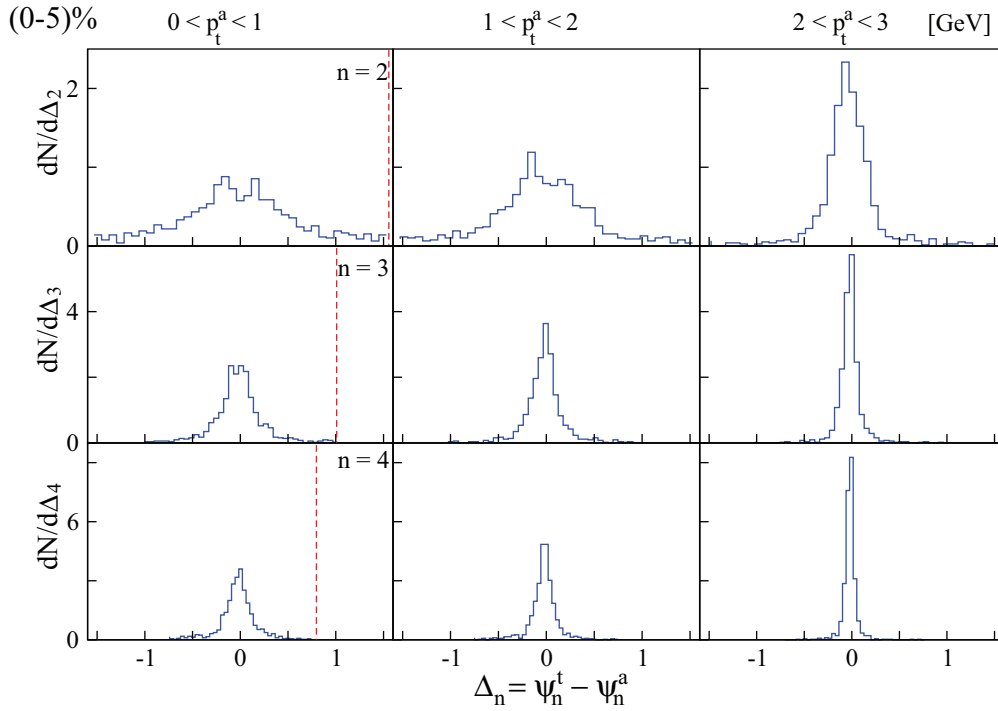


FIG. 6. (Color online) Distribution of the phase difference  $\Delta_n = \Psi_n^t - \Psi_n^a$  ( $n = 2, 3, 4$ ) in the 0–5% centrality window after 1000 events. Three ranges of transverse momentum, for associated particles, are presented. All distributions are normalized to 1. The vertical dashed line indicates the maximal difference for each harmonic, i.e.,  $\Delta_n^{\max} = \pi/n$ . The range in transverse momentum for the triggers is defined as  $3 < p_t^{\text{trigg}} < 5$  GeV.

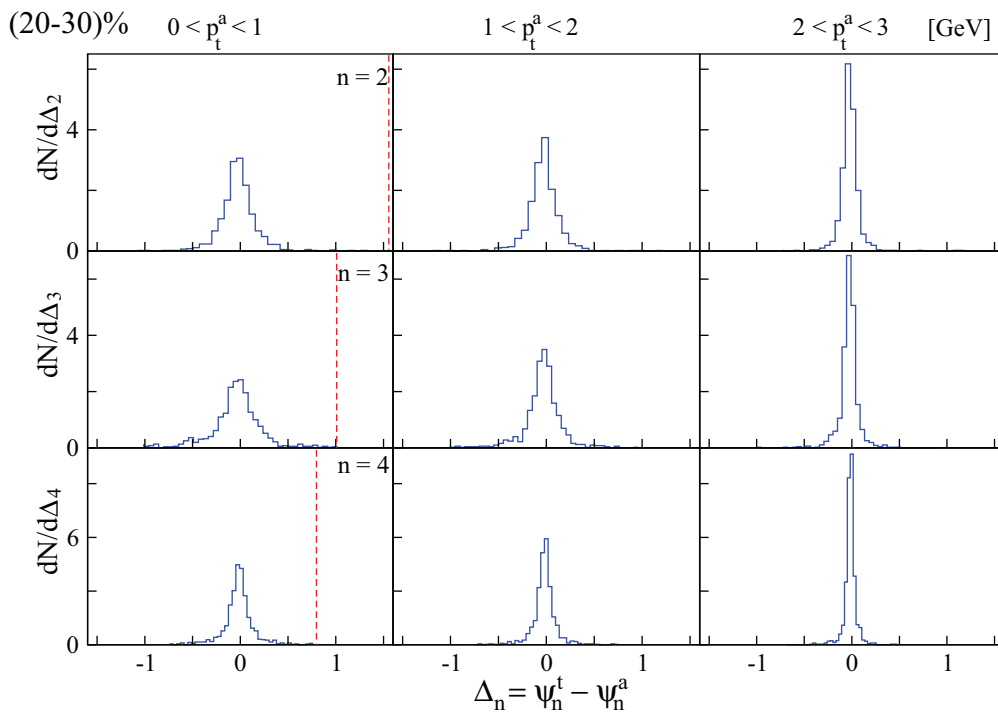


FIG. 7. (Color online) Distribution of the phase difference  $\Delta_n = \Psi_n^t - \Psi_n^a$  ( $n = 2, 3, 4$ ) in the 20–30% centrality window after 100 events. Three ranges of transverse momentum, for associated particles, are presented. All distributions are normalized to 1. The vertical dashed line indicates the maximal difference for each harmonic, i.e.,  $\Delta_n^{\max} = \pi/n$ . The range in transverse momentum for the triggers is defined as  $3 < p_t^{\text{trigg}} < 5$  GeV.

TABLE I. Average of the factors  $\langle \cos(n\Delta_n) \rangle$  and  $\langle \sin(n\Delta_n) \rangle$  for three ranges of transverse momentum of the associated particles in the 0–5% centrality window after 1000 events. The range in transverse momentum for the triggers is defined as  $3 < p_t^{\text{trigg}} < 5$  GeV. The first seven harmonics are shown.

$\langle \cos(n\Delta_n) \rangle$	$0 < p_t^a < 1$	$1 < p_t^a < 2$	$2 < p_t^a < 3$
$n = 1$	-0.741	0.809	0.969
$n = 2$	0.456	0.578	0.848
$n = 3$	0.766	0.842	0.932
$n = 4$	0.766	0.857	0.955
$n = 5$	0.759	0.836	0.956
$n = 6$	0.811	0.861	0.952
$n = 7$	0.842	0.875	0.957
$\langle \sin(n\Delta_n) \rangle$	$0 < p_t^a < 1$	$1 < p_t^a < 2$	$2 < p_t^a < 3$
$n = 1$	-0.020	0.002	0.005
$n = 2$	-0.004	0.011	0.004
$n = 3$	-0.004	-0.007	-0.009
$n = 4$	0.012	0.020	0.012
$n = 5$	0.010	0.012	0.005
$n = 6$	0.004	0.001	0.003
$n = 7$	-0.016	-0.009	-0.001

TABLE II. Average of the factors  $\langle \cos(n\Delta_n) \rangle$  and  $\langle \sin(n\Delta_n) \rangle$  for three ranges of transverse momentum of the associated particles in the 20–30% centrality window after 1000 events. The range in transverse momentum for the triggers is defined as  $3 < p_t^{\text{trigg}} < 5$  GeV. The first seven harmonics are shown.

$\langle \cos(n\Delta_n) \rangle$	$0 < p_t^a < 1$	$1 < p_t^a < 2$	$2 < p_t^a < 3$
$n = 1$	-0.721	0.709	0.940
$n = 2$	0.931	0.946	0.977
$n = 3$	0.747	0.850	0.954
$n = 4$	0.823	0.889	0.964
$n = 5$	0.860	0.906	0.971
$n = 6$	0.877	0.907	0.969
$n = 7$	0.899	0.921	0.967
$\langle \sin(n\Delta_n) \rangle$	$0 < p_t^a < 1$	$1 < p_t^a < 2$	$2 < p_t^a < 3$
$n = 1$	-0.031	0.027	0.013
$n = 2$	-0.011	-0.008	-0.006
$n = 3$	0.022	0.023	0.013
$n = 4$	-0.003	0.000	0.005
$n = 5$	-0.014	-0.010	-0.006
$n = 6$	-0.013	-0.011	-0.004
$n = 7$	0.005	0.003	0.002

We show in Table I the average of the factors  $\langle \cos(n\Delta_n) \rangle$  and  $\langle \sin(n\Delta_n) \rangle$  for the first seven harmonics, within three ranges of transverse momentum of the associated particles, in the 0–5% centrality window. Table II shows the same quantities for the 20–30% centrality window. The values in both tables are related to the width of the distributions that are shown in Figs. 6 and 7, respectively.

As one can see from the tables, the sine factors average to zero, as expected. This means that both the relative phase distribution and the di-hadron correlation function are even functions. With respect to the cosine factors, the absolute values are smaller than the unit as a consequence

of the fluctuations. The remarkable case occurs for associated particles with low transverse momentum ( $0 < p_t^a < 1$  GeV) in the 0–5% centrality window where  $\langle \cos(2\Delta_2) \rangle = 0.456$ . The negative signal that appears associated with the first harmonic is a consequence of the conservation of the momentum in the transverse plane—if the associated particles move in one direction, the triggers must move in the opposite direction to conserve momentum.

In Fig. 8 we show the total di-hadron correlation function  $C(\Delta\phi)$  and the corresponding background-subtracted function  $R(\Delta\phi)$  for three ranges of transverse momentum of the associated particles. The range in transverse momentum for

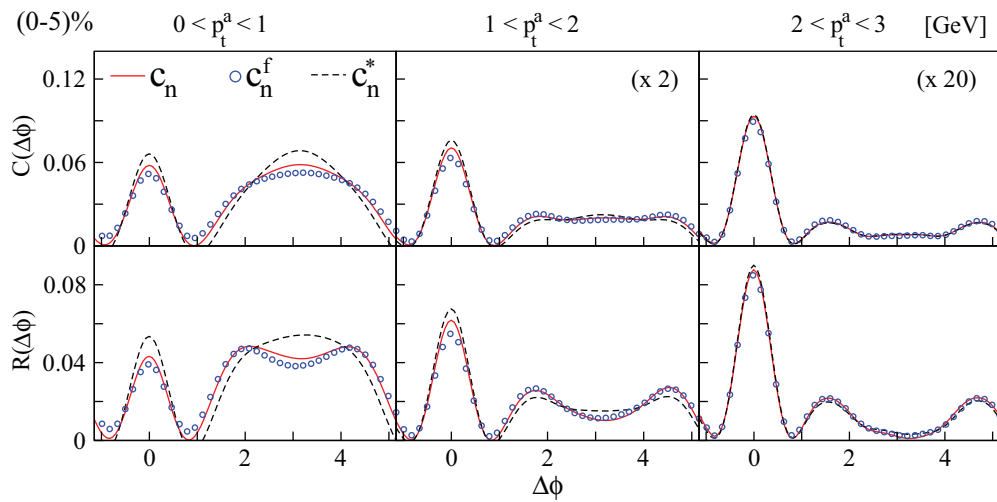


FIG. 8. (Color online) Total di-hadron correlation function  $C(\Delta\phi)$  (upper panels) and the corresponding background-subtracted correlation function  $R(\Delta\phi)$  (lower panels) for three ranges of transverse momentum of the associated particles in the 0–5% centrality window after 1000 events. The range in transverse momentum for the triggers is defined as  $3 < p_t^{\text{trigg}} < 5$  GeV. The solid lines correspond to the formulas in Eqs. (6) and (7) ( $c_n$ ); the lines with circles correspond to the factorized formula (8) ( $c_n^f$ ), and analogously for the sine terms; and the dashed lines correspond to formulas (6) and (7) without the cosine and sine factors, respectively, ( $c_n^*$ ).

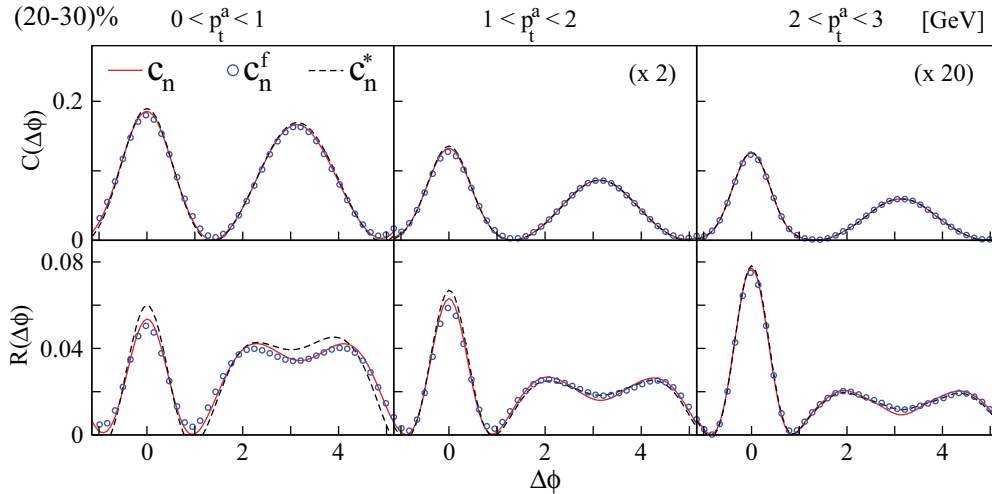


FIG. 9. (Color online) Total di-hadron correlation function  $C(\Delta\phi)$  (upper panels) and the corresponding background-subtracted correlation function  $R(\Delta\phi)$  (lower panels) for three ranges of transverse momentum of the associated particles in the 20–30% centrality window after 1000 events. The range in transverse momentum for the triggers is defined as  $3 < p_t^{\text{trigg}} < 5$  GeV. The solid lines correspond to the formulas in Eqs. (6) and (7) ( $c_n$ ); the lines with circles correspond to the factorized formula (8) ( $c_n^f$ ), and analogously for the sine terms; and the dashed lines correspond to formulas (6) and (7) without the cosine and sine factors, respectively, ( $c_n^*$ ).

the triggers is kept the same as before. A similar plot is shown in Fig. 9 for the (20–30)% centrality window. The solid lines correspond to the formulas in Eqs. (6) and (7) ( $c_n$ ); the lines with circles correspond to the factorized formula (8) ( $c_n^f$ ), and analogously for the sine terms; and the dashed lines correspond to formulas (6) and (7) without the cosine and sine factors, respectively, ( $c_n^*$ ).

The method that we used to remove the background and define the function  $R(\Delta\phi)$  is a variation of the widely known mixed event method (this was also used in Ref. [19]). In this method, the associated particles and the triggers are chosen in different events, producing a mixed correlation. This is usually used to remove the longitudinal correlation that arises from the shape of the longitudinal distribution of particles. In our version of this method, the events, which will be mixed, are aligned according to the direction of the event plane  $\Psi_2^{\text{EP}}$ . This procedure creates a background of the form  $c_2^{\text{mix}} \cos(2\Delta\phi)$ .

One can see from Figs. 8 and 9 that the fluctuation of the relative phases can change the shape of the di-hadron correlation function and the effect becomes more significant when the associated particles are chosen with low transverse momentum in comparison to the triggers. Observe that the factorized formula is already a reasonable approximation of the original formulas, Eqs. (6) and (7), after 1000 events.

## VI. CONCLUSIONS

In this paper, we studied the di-hadron angular correlation function within boost-invariant, ideal hydrodynamics for Au + Au collisions at  $\sqrt{s_{NN}} = 200$  GeV using Monte Carlo Glauber fluctuating initial conditions. We observed, when  $0 < p_T < 3$  GeV, that the intensity of the flow components and their phases,  $\{v_n, \Psi_n\}$  ( $n = 2, 3$ ), are found to be correlated on an event-by-event basis with the initial condition geometrical parameters  $\{\varepsilon_{2,n}, \Phi_{2,n}\}$ , respectively. More precisely, we have

found that there is a considerable linear correlation between  $v_n$  and  $\varepsilon_{2,n}$  ( $n = 2, 3$ ), for three different  $p_T$  bins, both in central and peripheral collisions. In addition, we have shown that the phase that defines each flow component,  $\Psi_n$ , is partially aligned with the respective reference angle  $\Phi_{2,n}$ , for three different  $p_T$  bins (when  $0 < p_T < 3$  GeV), both in central and peripheral collisions. We found that  $\Psi_4$  remains generally aligned to  $\Phi_{2,4}$  even though  $v_4$  and  $\varepsilon_{2,4}$  are not strongly linearly correlated. These results show that, considering low and moderate  $p_T$ , the nonlinear hydrodynamic evolution indeed preserves the global geometric parameters that characterize the initial conditions event by event. In the case of high transverse momentum ( $3 < p_T < 5$  GeV), the  $\delta_2$  distribution computed in the 0–5% centrality window is considerably broad.

The phase difference between trigger and associated hadrons,  $\Delta_n = \Psi_n^t - \Psi_n^a$ , which is, in principle, nonzero when both angles are defined using different  $p_T$  bins, can affect the di-hadron angular correlation function. The remarkable case occurs in the 0–5% centrality window when the triggers are taken in the interval  $3 < p_T < 5$  GeV and the associated particles are taken in the interval  $0 < p_T < 1$  GeV. Once the associated particles are aligned with the reference angle  $\Phi_{2,n}$  and the triggers are not, the factor  $\langle \cos(2\Delta_2) \rangle$  is rather smaller than the unit ( $\sim 0.456$ ). Consequently, according to the Eq. (6), this result reduces the contribution of the second harmonic to the di-hadron correlation function. Moreover, we have found (after 1000 events) that the final angular correlation function,  $C(\Delta\phi)$ , and its background-subtracted version,  $R(\Delta\phi)$ , are even functions of  $\Delta\phi$ . This is a consequence of the parity property of the relative phase distributions  $\Delta_n$ .

## ACKNOWLEDGMENTS

R. P. G. Andrade and J. Noronha acknowledge Fundação de Amparo à Pesquisa do Estado de São Paulo (FAPESP) and

Conselho Nacional de Desenvolvimento Científico e Tecnológico (CNPq) for financial support. The authors thank G. S. Denicol, Y. Hama, F. Grassi, F. Gardim, M. Luzum, and J.-Y. Ollitrault for discussions on the hydrodynamic description of di-hadron angular correlations and A. Dumitru for providing the Monte Carlo Glauber model.

### APPENDIX A: THE SPH METHOD

The SPH formulation of relativistic inviscid hydrodynamics can be done in terms of the variational principle [38,46]. For the sake of completeness, we review this formulation below. We start with the Lagrangian formulation of the relativistic hydrodynamics, in the approximation of an ideal fluid, for vanishing baryon chemical potential. Such a formulation is done by the action

$$I = - \int \epsilon[s(\vec{x}, x^0)] \sqrt{-g} d^4x, \quad (\text{A1})$$

under the constraints

$$(su^v)_{;v} = \frac{1}{\sqrt{-g}} \partial_v (\sqrt{-g} s u^v) = 0 \quad (\text{A2})$$

and

$$u^\mu u_\mu = 1, \quad (\text{A3})$$

where  $\epsilon$  and  $s$  are the energy density and the entropy density of the fluid, respectively (in the local frame),  $x = (x^0, x^1, x^2, x^3)$  is the generalized coordinate,  $g$  is the determinant of the metric tensor,  $g_{\mu\nu}$ , and  $\sqrt{-g}$  is the Jacobian determinant. We consider only metrics of the following form

$$(g_{\mu\nu}) = \begin{bmatrix} g_{00} & 0 \\ 0 & -\mathbf{g} \end{bmatrix}, \quad (\text{A4})$$

where  $\mathbf{g}$  is the spatial part of the metric tensor (a  $3 \times 3$  matrix).

By using formulas (A3) and (A4), one finds that

$$\gamma = \frac{1}{\sqrt{g_{00} - [\vec{v}]^T \mathbf{g} \vec{v}}} \quad (\text{A5})$$

where  $v^i = u^i/u^0$ .

Having depicted the Lagrangian formalism for the ideal relativistic hydrodynamics, let us introduce the concepts of the SPH method. The basic idea of this method is to parametrize the density of the extensive thermodynamic quantities, each density associated with a conserved charge, in the following way:

$$a^*(\vec{x}, x^0) = \sum_{j=1}^N v_j W(\vec{x} - \vec{x}_j(x^0); h), \quad (\text{A6})$$

where the density  $a^*$  is associated with an extensive quantity  $\mathcal{A}$  and is measured in a space-fixed (calculational) frame. The weights  $v_j$  are defined by the initial conditions and their values are kept constant during the hydrodynamic expansion.  $W$  is a positive-definite function called the kernel function defined using a length scale  $h$  called the SPH smoothing parameter

and this function has the following properties:

$$W(\vec{x} - \vec{x}_j(x^0); h) = W(\vec{x}_j(x^0) - \vec{x}; h), \quad (\text{A7})$$

$$\int W(\vec{x} - \vec{x}_j(x^0); h) d^3\vec{x} = 1, \quad (\text{A8})$$

and

$$\lim_{h \rightarrow 0} W(\vec{x} - \vec{x}_j(x^0); h) = \delta^3(\vec{x} - \vec{x}_j(x^0)). \quad (\text{A9})$$

Usually, the coordinates  $\vec{x}_j$ , which explicitly depend on the “time”  $x^0$ , are called SPH Lagrangian coordinates or simply SPH particles. Each one carries a portion  $v_j$  of the extensive quantity  $\mathcal{A}$ .

Considering that

$$a^* \rightarrow s^* = \sqrt{-g} \gamma s \quad (\text{A10})$$

and

$$\vec{v}(\vec{x}, x^0) \equiv \frac{1}{s^*} \sum_{j=1}^N v_j \frac{d\vec{x}}{dx^0} W(\vec{x} - \vec{x}_j(x^0); h), \quad (\text{A11})$$

it is not difficult to realize that the parametrization (A6) satisfies the constraints (A2) and (A3), independently on the motion of the SPH particles. This is one of the advantages of this method: the entropy is automatically conserved throughout the whole time evolution. Thus, the equation of motion for each one of the SPH particles is obtained from the condition  $\delta I = 0$ .

It is convenient at this point to define the following notation:

$$s_i^* = (\sqrt{-g})_i \gamma_i s_i. \quad (\text{A12})$$

The subscript index indicates that the physical quantity must be computed at the position of the  $i$ th SPH particle, i.e.,  $\vec{x} = \vec{x}_i$ . Keeping this notation in mind, the energy density profile can be parameterized as follows:

$$\epsilon(\vec{x}, x^0) = \sum_{j=1}^N \epsilon_j \left( \frac{v_j}{s_j^*} \right) W(\vec{x} - \vec{x}_j(x^0); h). \quad (\text{A13})$$

The quantity  $V^* = (v_j/s_j^*)$  is usually called the SPH particle volume. Observe that the extensive thermodynamic quantity used to define the SPH particle volume cannot vanish. This makes the entropy a convenient choice in the case of an ideal fluid. In the case where viscous effects are included and, hence, there is entropy production, a different conserved quantity is chosen to define the SPH particle volume [47,48].

Introducing the parametrization (A13) in the action (A1) one finds that

$$I \rightarrow I_{\text{SPH}} = - \sum_{j=1}^N \int \frac{E_j}{\gamma_j} d\tau, \quad (\text{A14})$$

where  $E_j = \epsilon_j V_j$  and  $V_j = (v_j/s_j^*)$  is the proper volume of the SPH particle.

Taking into account that  $\delta E_j = -p_j \delta V_j$ , where  $p_j$  is the pressure of the fluid, the condition  $\delta I_{\text{SPH}} = 0$  leads to the following set of ordinary differential equations in the

hyperbolic coordinate system:

$$\begin{aligned} & \frac{d}{d\tau} \begin{pmatrix} \vec{\pi}_T \\ \vec{\pi}_\eta \end{pmatrix}_i \\ &= - \sum_{j=1}^N \frac{v_i v_j}{\tau} \left( \frac{p_i}{(\gamma_i s_i)^2} + \frac{p_j}{(\gamma_j s_j)^2} \right) \begin{pmatrix} \nabla_T \\ \partial_\eta \end{pmatrix}_i W_{ij}, \end{aligned} \quad (\text{A15})$$

where

$$(\vec{\pi}_T)_i = v_i \gamma_i \left( \frac{\epsilon_i + p_i}{s_i} \right) (\vec{v}_T)_i, \quad (\text{A16})$$

$$(\vec{\pi}_\eta)_i = \tau^2 v_i \gamma_i \left( \frac{\epsilon_i + p_i}{s_i} \right) (v_\eta)_i, \quad (\text{A17})$$

$$\gamma_i = (1 - (\vec{v}_T)_i^2 - \tau^2 (v_\eta)_i^2)^{-\frac{1}{2}}, \quad (\text{A18})$$

$$(\nabla_T)_i = (\partial_x, \partial_y)_i, \quad (\text{A19})$$

and

$$W_{ij} = W((\vec{r}_T)_i - (\vec{r}_T)_j, \eta_i - \eta_j; h). \quad (\text{A20})$$

In Eqs. (A15)–(A20):  $(\vec{v}_T)_i = (d\vec{r}_T/d\tau)_i$ ,  $(v_\eta)_i = (d\eta/d\tau)_i$ ,  $\tau = \sqrt{t^2 - z^2}$ ,  $\eta = 0.5 \ln[(t+z)/(t-z)]$ , and  $\vec{r}_T = (x, y)$ .

Thus, one can see that a feature of the SPH approach is that the dynamics of the relativistic fluid is described by a set of ordinary differential equations whose solutions can be obtained by simple numerical methods.

In the boost-invariant ansatz, it is not difficult to realize that the longitudinal equation is trivially satisfied, once  $v_\eta = 0$  and the pressure gradient vanishes along the  $\eta$  direction. Moreover, in this solution

$$W((\vec{r}_T)_i - (\vec{r}_T)_j, \eta_i - \eta_j; h) \rightarrow W((\vec{r}_T)_i - (\vec{r}_T)_j; h), \quad (\text{A21})$$

because the transverse flow is identical in any transverse plane.

### 1. Numerical parameters

In the SPH method there are three basic parameters that determine the dynamics of each SPH particle: the width of the  $W$  function,  $h$ ; the total number of SPH particles,  $N$ ; and the size of the time step  $d\tau$  used in the numerical solution of the ordinary differential equations (A15). The parameter  $h$  fixes the resolution of the interpolation formula (A6); i.e., the smaller is  $h$ , the more detailed the profile of the density  $a^*$  is. The parameter  $N$ , taking into account the fact that the SPH particles move together with the fluid, must be large enough to guarantee a minimal number of SPH particles inside an arbitrary area  $\delta A \approx \pi h^2$  (in the case of a three-dimensional calculation, an arbitrary volume should be considered). In other words: for a fixed  $h$ , the hydrodynamic solution should not depend on the parameter  $N$ . In general, for a given  $h$  one increases  $N$  until the quantities computed become insensitive to further changes in this parameter.

In this work,  $h = 0.3$  fm,  $N \sim 70\,000$ , and  $d\tau = 0.1$  fm are used. This choice for  $h$  preserves all the interesting structure present in the initial conditions and this value of  $N$  is large enough to guarantee convergence of the results computed in this paper. By using these parameters, the relative error in the

total energy conservation, comparing the energy at beginning of the simulation with the energy at the end, is smaller than 0.1%. For two consecutive steps, the relative error is smaller than 0.001%.

## APPENDIX B: GUBSER FLOW

The analytical solution obtained by Gubser for the transverse flow (azimuthally symmetric) of a boost-invariant, ideal and conformal ( $\epsilon = 3p$ ) fluid is the following [39]:

$$\epsilon(\tau, r) = \frac{\epsilon_0 (2q)^{\frac{8}{3}}}{\tau^{\frac{4}{3}} [1 + 2q^2(\tau^2 + r^2) + q^4(\tau^2 - r^2)^2]^{\frac{4}{3}}} \quad (\text{B1})$$

and

$$v_T(\tau, r) = \tanh[\kappa(\tau, r)] = \frac{2q^2 \tau r}{1 + q^2 \tau^2 + q^2 r^2}, \quad (\text{B2})$$

where  $v_T$  is the transverse velocity;  $q$  is an arbitrary parameter (with dimension  $\text{fm}^{-1}$ ), which is related to the transverse distribution of matter; and  $\epsilon_0$  is a dimensionless normalization factor.

In Fig. 10 we show the comparison between the exact solution and our numerical computation for the energy density distribution and transverse four-velocity ( $u_T = \sinh \kappa$ ), both quantities as functions of the transverse radius coordinate  $r$ . For the sake of simplicity,  $\epsilon_0 = 1$  and  $q = 1 \text{ fm}^{-1}$  are used. As one can see, the code reproduces the exact solution with great accuracy.

## APPENDIX C: COOPER-FRYE PRESCRIPTION IN THE SPH APPROACH

In the Cooper-Frye prescription [44] the invariant momentum distribution is given by

$$E \frac{dN}{d^3 \vec{p}} = \frac{g}{(2\pi)^3} \int_\Sigma f(T_{i0}, p^\nu u_\nu) p^\mu d\sigma_\mu, \quad (\text{C1})$$

where  $f$  is the particle distribution as a function of the momentum  $\vec{p}$ . We have assumed zero baryon chemical potential. The integral is done on the hypersurface  $\Sigma$ , characterized by a constant temperature (the freeze-out temperature  $T_{i0}$ ). In the case of ideal hydrodynamics,  $f$  is the thermal equilibrium distribution.

In the SPH representation (see Appendix A), the Cooper-Frye formula (C1) becomes [49]

$$E \frac{dN}{d^3 \vec{p}} = \sum_{j=1}^N p^\nu(q_\nu)_j f_j, \quad (\text{C2})$$

where

$$(q_\nu)_j = \frac{g}{(2\pi)^3} \frac{(n_\nu)_j}{|(n_\mu)_j (u^\mu)_j|} \frac{v_j}{s_j}, \quad (\text{C3})$$

and

$$f_j = \frac{1}{\exp[p^\nu (u_\nu)_j / T_{i0}] \pm 1}. \quad (\text{C4})$$

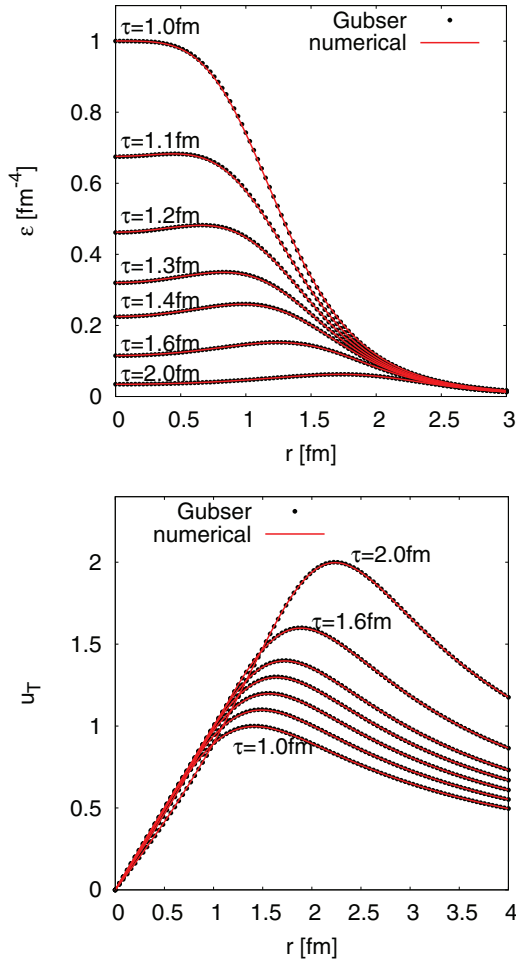


FIG. 10. (Color online) Energy density distribution and transverse four-velocity ( $u_T = \sinh \kappa$ ) defined as a function of the transverse radius  $r$ . The dots represent the exact solution and the solid lines the numerical computation. We used  $\epsilon_0 = 1$  and  $q = 1 \text{ fm}^{-1}$ .

In formula (C2), the summation is over all SPH particles. The quantities with the index  $j$  must be computed at the position of the  $j$ th SPH particle when it achieves the freeze-out hypersurface  $\Sigma$ . The quantity  $(n_\nu)_j$  is the normal to this hypersurface.

Formula (C2) in the hyperbolic coordinate system can be put in the following form

$$\frac{dN}{dp^x dp^y dp^\eta} = \sum_{j=1}^N f_j \left[ \tau (q_\tau)_j - \tau \frac{\vec{p}_T \cdot (\vec{q}_T)_j}{p^\tau} \right], \quad (\text{C5})$$

where

$$f_j = \frac{1}{\Lambda_j \exp[p^\tau (u^\tau)_j / T_{f0}] \pm 1}, \quad (\text{C6})$$

$\vec{p}_T = (p^x, p^y)$ , and  $\Lambda_j = e^{-\vec{p}_T \cdot (\vec{u}_T)_j / T_{f0}}$ . In Eq. (C5), we used  $\eta = 0$  (the computation is done at the midrapidity) and  $(q_\eta)_j = 0$  (in the boost invariant solution the normal to the hypersurface  $\Sigma$  does not have a longitudinal component). In Eq. (C6), we used  $u^\eta = 0$  (longitudinal boost-invariant flow).

The distribution of particles as a function of the transverse momentum can be obtained by the integration of Eq. (C5) with respect to the longitudinal momentum  $p^\eta$ . In this kind of calculation, the SPH particles are placed only in one transverse plane: the midrapidity transverse plane, once the transverse hydrodynamic evolution is boost invariant. This integration takes into account this symmetry. Thus,

$$\frac{dN}{dp^x dp^y} = \sum_{j=1}^N [(q_\tau)_j m_T (I_2^\pm)_j - \vec{p}_T \cdot (\vec{q}_T)_j (I_1^\pm)_j], \quad (\text{C7})$$

where

$$(I_1^\pm)_j = \int_{-\infty}^{\infty} \frac{(1+x^2)^{-\frac{1}{2}}}{\Lambda_j \exp[\sigma_j \sqrt{1+x^2}] \pm 1} dx, \quad (\text{C8})$$

$$(I_2^\pm)_j = \int_{-\infty}^{\infty} \frac{1}{\Lambda_j \exp[\sigma_j \sqrt{1+x^2}] \pm 1} dx, \quad (\text{C9})$$

$(\vec{q}_T)_j = (q^x, q^y)_j$ ,  $m_T = \sqrt{\vec{p}_T \cdot \vec{p}_T + m^2}$  is the transverse mass, and  $\sigma_j = m_T (u^\tau)_j / T_{f0}$ .

By using the integral form of the modified Bessel functions  $K_\nu$ , the integrals (C8) and (C9) can be written as

$$(I_1^+)_j = \sum_{n=1}^{\infty} (-1)^{n+1} \frac{2}{(\Lambda_j)^n} K_0(n\sigma_j), \quad (\text{C10})$$

$$(I_1^-)_j = \sum_{n=1}^{\infty} \frac{2}{(\Lambda_j)^n} K_0(n\sigma_j), \quad (\text{C11})$$

$$(I_2^+)_j = \sum_{n=1}^{\infty} (-1)^{n+1} \frac{2}{(\Lambda_j)^n} K_1(n\sigma_j), \quad (\text{C12})$$

and

$$(I_2^-)_j = \sum_{n=1}^{\infty} \frac{2}{(\Lambda_j)^n} K_1(n\sigma_j). \quad (\text{C13})$$

Finally, it is important to mention that in this approach there is an interval around midrapidity that is implicitly defined when the entropy portion  $v_j$  is assigned to the SPH particles at the beginning of the simulation [see Eqs. (A6) and (A10)].

- [1] J. Adams *et al.* (STAR Collaboration), *Phys. Rev. Lett.* **95**, 152301 (2005).  
 [2] A. Adare *et al.* (PHENIX Collaboration), *Phys. Rev. C* **78**, 014901 (2008).  
 [3] B. Abelev *et al.* (STAR Collaboration), *Phys. Rev. C* **80**, 064912 (2009).

- [4] S. Chatrchyan *et al.* (CMS Collaboration), *J. High Energy Phys.* **07** (2011) 076.  
 [5] V. Khachatryan *et al.* (CMS Collaboration), *J. High Energy Phys.* **09** (2010) 091.  
 [6] S. Chatrchyan *et al.* (CMS Collaboration), *Phys. Lett. B* **718**, 795 (2013).

- [7] H. Stoecker, *Nucl. Phys. A* **750**, 121 (2005).
- [8] J. Casalderrey-Solana, E. Shuryak, and D. Teaney, *J. Phys. Conf. Ser.* **27**, 22 (2005).
- [9] L. Satarov, H. Stoecker, and I. Mishustin, *Phys. Lett. B* **627**, 64 (2005).
- [10] A. K. Chaudhuri and U. Heinz, *Phys. Rev. Lett.* **97**, 062301 (2006).
- [11] T. Renk, *Phys. Rev. C* **78**, 014903 (2008).
- [12] J. Noronha, M. Gyulassy, and G. Torrieri, *Phys. Rev. Lett.* **102**, 102301 (2009).
- [13] B. Betz, M. Gyulassy, J. Noronha, and G. Torrieri, *Phys. Lett. B* **675**, 340 (2009).
- [14] B. Betz, J. Noronha, G. Torrieri, M. Gyulassy, I. Mishustin, and D. H. Rischke, *Phys. Rev. C* **79**, 034902 (2009).
- [15] G. Torrieri, B. Betz, J. Noronha, and M. Gyulassy, *Acta Phys. Pol. B* **39**, 3281 (2008).
- [16] B. Betz, J. Noronha, G. Torrieri, M. Gyulassy, and D. H. Rischke, *Phys. Rev. Lett.* **105**, 222301 (2010).
- [17] R. P. G. Andrade, F. Grassi, Y. Hama, T. Kodama, and W. L. Qian, *Phys. Rev. Lett.* **101**, 112301 (2008).
- [18] R. Andrade, F. Grassi, Y. Hama, T. Kodama, and O. Socolowski, Jr., *Phys. Rev. Lett.* **97**, 202302 (2006).
- [19] J. Takahashi, B. M. Tavares, W. L. Qian, R. Andrade, F. Grassi, Y. Hama, T. Kodama, and N. Xu, *Phys. Rev. Lett.* **103**, 242301 (2009).
- [20] B. Alver and G. Roland, *Phys. Rev. C* **81**, 054905 (2010).
- [21] B. H. Alver, C. Gombeaud, M. Luzum, and J.-Y. Ollitrault, *Phys. Rev. C* **82**, 034913 (2010).
- [22] R. S. Bhalerao, M. Luzum, and J.-Y. Ollitrault, *Phys. Rev. C* **84**, 054901 (2011).
- [23] R. S. Bhalerao, M. Luzum, and J.-Y. Ollitrault, *Phys. Rev. C* **84**, 034910 (2011).
- [24] D. Teaney and L. Yan, *Phys. Rev. C* **83**, 064904 (2011).
- [25] G.-Y. Qin, H. Petersen, S. A. Bass, and B. Muller, *Phys. Rev. C* **82**, 064903 (2010).
- [26] F. G. Gardim, F. Grassi, M. Luzum, and J.-Y. Ollitrault, *Phys. Rev. C* **85**, 024908 (2012).
- [27] B. Alver *et al.* (PHOBOS Collaboration), *Phys. Rev. Lett.* **98**, 242302 (2007).
- [28] Z. Qiu and U. W. Heinz, *Phys. Rev. C* **84**, 024911 (2011).
- [29] H. Niemi, G. S. Denicol, H. Holopainen, and P. Huovinen, *Phys. Rev. C* **87**, 054901 (2013).
- [30] D. Teaney and L. Yan, *Phys. Rev. C* **86**, 044908 (2012).
- [31] F. G. Gardim, F. Grassi, M. Luzum, and J.-Y. Ollitrault, *Phys. Rev. C* **87**, 031901 (2013).
- [32] U. W. Heinz, Z. Qiu, and C. Shen, *Phys. Rev. C* **87**, 034913 (2013).
- [33] Z. Qiu and U. Heinz, *Phys. Lett. B* **717**, 261 (2012).
- [34] F. G. Gardim, Y. Hama, and F. Grassi, *Prog. Theor. Phys. Suppl.* **193**, 319 (2012).
- [35] A. M. Poskanzer and S. A. Voloshin, *Phys. Rev. C* **58**, 1671 (1998).
- [36] Y. Hama, T. Kodama, and O. Socolowski, Jr., *Braz. J. Phys.* **35**, 24 (2005).
- [37] J. D. Bjorken, *Phys. Rev. D* **27**, 140 (1983).
- [38] C. E. Aguiar, T. Kodama, T. Osada, and Y. Hama, *J. Phys. G* **27**, 75 (2001).
- [39] S. S. Gubser, *Phys. Rev. D* **82**, 085027 (2010).
- [40] H.-J. Drescher and Y. Nara, *Phys. Rev. C* **75**, 034905 (2007).
- [41] H.-J. Drescher and Y. Nara, *Phys. Rev. C* **76**, 041903 (2007).
- [42] M. Luzum, C. Gombeaud, and J.-Y. Ollitrault, *Phys. Rev. C* **81**, 054910 (2010).
- [43] P. Huovinen and P. Petreczky, *Nucl. Phys. A* **837**, 26 (2010).
- [44] F. Cooper and G. Frye, *Phys. Rev. D* **10**, 186 (1974).
- [45] P. Mota, T. Kodama, R. Derradi de Souza, and J. Takahashi, *Eur. Phys. J. A* **48**, 165 (2012).
- [46] H.-T. Elze, Y. Hama, T. Kodama, M. Makler, and J. Rafelski, *J. Phys. G* **25**, 1935 (1999).
- [47] G. S. Denicol, T. Kodama, T. Koide, and P. Mota, *Phys. Rev. C* **80**, 064901 (2009).
- [48] J. Noronha-Hostler, G. S. Denicol, J. Noronha, R. P. G. Andrade, and F. Grassi, [arXiv:1305.1981](https://arxiv.org/abs/1305.1981).
- [49] T. Osada, C. Aguiar, Y. Hama, and T. Kodama, [arXiv:nucl-th/0102011](https://arxiv.org/abs/nucl-th/0102011).